Performance Characteristics of a MEMS Quadrupole Mass Filter With Square Electrodes: Experimental and Simulated Results

Performance Characteristics of a MEMS Quadrupole Mass Filter With Square Electrodes: Experimental and Simulated Results

Thomas J. Hogan, *Member, IEEE*, Stephen Taylor, Kerry Cheung, Luis Fernando Velásquez-García, *Member, IEEE*, Akintunde Ibitayo Akinwande, *Fellow, IEEE*, and Randall E. Pedder

***Abstract*—Size reduction in quadrupole mass spectrometers (QMSs) is an ongoing requirement driven by the needs of space exploration, portable, and covert monitoring applications. Microelectromechanical systems (MEMS) technology provides a method of achieving this size reduction. A quadrupole mass filter (QMF) is one component of a QMS and is suitable for microfabrication. MEMS manufacturing techniques are more suitable to the production of rectilinear electrodes, instead of the more widely used circular electrodes. Present understanding of the performance characteristics of rectilinear electrodes and the dependence of these characteristics on electrode geometry are not well documented. In this paper, we report on the performance characteristics of a square-electrode QMF. Both the predicted performances obtained by computer simulation and experimental data are presented for operation in stability zone 1 (0.236, 0.706) and zone 3 (3.16, 3.23). A comparison between these results and the simulated data for equivalent devices constructed using hyperbolic and circular electrodes for operation in zone 1 is also made. This comparison demonstrates that, although the field produced by square electrodes is far from the "ideal," it is still possible to achieve useful filtering action. Our results also show that, for operation in zone 3, performance comparable with that of hyperbolic and circular electrodes operating in zone 1 is achievable.**

***Index Terms*—Microelectromechanical, multipoles, quadrupole mass filter, square electrode, zone 3.**

I. Introduction

A VERY CLOSE approximation to an ideal quadrupole mass filter (QMF) consists of four hyperbolic-shaped electrodes mounted inside a conductive enclosure. With positive and negative potentials of equal magnitude applied to alternate electrodes, a hyperbolic field is produced in the central field area between the electrodes [1], [2]. The cost and ease of manufacturing make circular electrodes the normal choice of instrument manufacturers. Circular electrodes produce a field that consists of a hyperbolic component (second order) with a number of higher order components superimposed, which is called a multipole field [3]–[5].

Manuscript received February 26, 2009; revised September 8, 2009; accepted September 28, 2009. Date of publication July 8, 2010; date of current version August 11, 2010. The Associate Editor coordinating the review process for this paper was Dr. Yves Rolain.

T. J. Hogan and S. Taylor are with the Department of Electrical Engineering and Electronics, University of Liverpool, L69 3BX Liverpool, U.K.

K. Cheung, L. F. Velásquez-García, and A. I. Akinwande are with Massachusetts Institute of Technology, Cambridge, MA 02139-4307 USA.

R. E. Pedder is with Ardara Technologies L.P., North Huntington, PA 15642 USA.

Digital Object Identifier 10.1109/TIM.2009.2036346

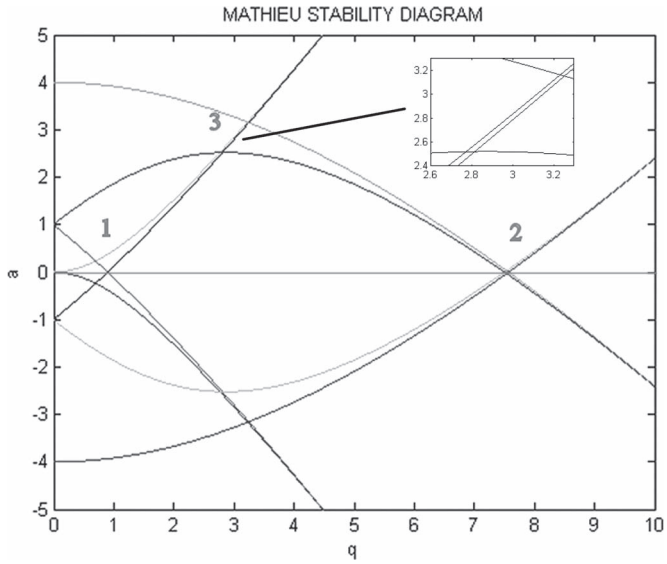

Fig. 1. Mathieu Stability diagram showing the first three stability zones, with the inset showing zone 3 in greater detail.

With the correct ratio of electrode radius r to central field radius r_0, a close approximation to the ideal hyperbolic field is achievable. Early research empirically ascribed an optimum value of r/r_0 to be 1.148 [6]. This was later refined by theoretical analysis to 1.1468 [7], where a zero value for the dodecapole term A_6 is achieved and which results in the closest approximation to a pure quadrupole field. The increasing power of modern personal computers has enabled the performance of a QMF to be investigated by numerical simulation of the trajectories of a large number of ions. These techniques have demonstrated that an r/r_0 ratio in the ranges of 1.120–1.130 [8], 1.125–1.130 [9], and ≈1.130 [4] results in an optimum performance from circular-electrode QMFs when operated in stability zone 1. This has also been confirmed to be the case for operation in stability zone 3 [10]. Fig. 1 shows the Mathieu Stability diagram with the first three stability zones identified and added detail for zone 3. These results show that the closest approximation to the quadrupole field does not provide the optimum QMF performance. This relationship has also been confirmed by analytical techniques [4], which show that an r/r_0 value in the range of 1.128–1.130 results in optimum performance, with these results being explained in terms of the A_6 and A_{10} multipole coefficients having opposite polarity and nearly equal magnitudes, producing an interaction of the

multipole field components such as to significantly cancel out their individual contributions.

For many applications, such as spaceborne research instrumentation, covert monitoring and portable applications, a reduction in size, operating vacuum pressure, and power is desirable and, in some cases, mandatory. Successful miniaturization of a quadrupole mass spectrometer (QMS) and, in particular, the QMF has previously been reported, and a variety of different implementations have been produced using circular electrodes [11]. An early example utilized metallized glass electrodes mounted on etched silicon mounts [12], [13]. More recently, precision-machined circular metal electrodes have been mounted on a monolithic block with etched features and springs to provide accurate location of the electrodes [14], [15]. Commercially available metal dowel pins with diameters ranging from 0.25 to 1.58 mm and mounted on a microfabricated platform have also been used to produce a QMF [16].

The use of microelectromechanical systems (MEMS) microfabrication techniques provides one method of achieving accurate high-volume manufacturing of a QMF. This manufacturing process is better suited to the construction of rectilinear-shaped electrodes. Novel electrode geometries have previously been reported and have been shown to generate electric fields that approximate to the quadrupole field. Hayashi and Sakudo [17] reported on the use of concave electrodes suitable for vacuum deposition and also the optimization of quadrupole electrodes with flat faces [18] to minimize the multipole field distortions. A little later, Pearce and Halsall [19] demonstrated that a quadrupole field accurate to 0.1% in a significant portion of the central region could be achieved with flat electrodes.

A micromachined Wein filter employing square electrodes for use as a low-cost leak detector [20], together with a patent for a square-electrode QMF [21], demonstrates an ongoing interest in square-electrode geometry.

It is well known that distortions to the quadrupole field of a QMF impacts performance [22]. To date, the application of high-ion-count numerical simulation techniques has been limited to the investigation of hyperbolic- [23] and circular-electrode devices [24]. These have shown that circular electrodes produce reduced transmission, low-mass tailing, and increased peak width when compared with hyperbolic electrodes.

The dependence of the multipole coefficients of square-electrode QMFs on electrode geometry and the resultant performance characteristics are not well documented. For a microengineered QMF constructed from circular electrodes, the effects of electrode to substrate distances are known to affect field asymmetries and, hence, the magnitude of the multipole field coefficients [12]. The previously reported optimization [25] of the square-electrode QMF used in these experiments demonstrated similar characteristics, finding that the optimum value for the electrode geometry was dependent on the distance of the electrode from the substrate and also on the ratio of the electrode size to the effective device aperture radius r_0. Table I shows the relative magnitudes of the multipole coefficients for the optimum rectilinear electrodes and for circular electrodes. It can be seen that there is a significant difference, i.e., the square electrodes result in a decrease of approximately 22% in the quadrupole coefficient A_2, with the next three higher terms all positive with much increased magnitudes. These significant differences suggest that there may well be a considerable degradation in the performance achieved from a QMF constructed with square electrodes.

TABLE I
MULTIPOLE COEFFICIENTS AT RADIUS r_0 FOR CIRCULAR- AND SQUARE-ELECTRODE GEOMETRIES EXTRACTED FROM POISSON FOR DIMENSIONS DEFINED IN TABLE II

A_N	CIRCULAR ELECTRODE	SQUARE ELECTRODE
2	1.0016E+00	0.78381E+00
6	1.2000E-03	8.0909E-02
10	-2.4325E-03	3.2235E-02
14	-2.9680E-04	1.8101E-02

The resolving quality of a QMF is dependent on the number of RF cycles [1], [26] that the ions experience during their passage through the filter. Reducing the physical size of a QMF results in a shorter ion path with a proportional reduction in the number of RF cycles experienced by the ion for a given RF frequency. The shorter ion path does however offer the advantage of enabling the QMF to be operated at higher pressures. The increased operating pressure relaxes the pumping requirement, allowing for the use of smaller and more portable vacuum systems. The combination of these key attributes for this class of device and the impact on performance was a driver for undertaking this study.

We report on the performance characteristics of a microfabricated QMF implemented with square electrodes [25] using simulations and experimental data. The device comprises five heavily doped silicon wafers that are patterned and bonded together. The device measures 15 mm $\times$ 4 mm $\times$ 35 mm and contains the housing, the quadrupole, and integrated optics (Fig. 2). Previously reported computer simulation techniques [10] have been used to obtain data for this MEMS device and to benchmark the performance characteristics of equivalent circular- and hyperbolic-electrode devices. Both low- and high-mass performances have been investigated to quantify any mass-dependent performance characteristics that may exist.

As with a traditionally manufactured QMF, MEMS process technologies have finite process tolerances, which can possibly result in degraded performance. The impact of these tolerances on the performance of traditionally constructed circular electrodes is documented, and acceptable tolerance limits have been defined [27], [28]. The effects of traditional tolerances and the most likely forms of MEMS process tolerances on the mass peak shape have been investigated through computer simulation, and these results are also included in this paper.

II. THEORY

Fig. 3(a) and (b) shows end views of a circular- and square-electrode QMF, respectively. To generate the correct electric field to achieve mass filtering action [1], [2], the x electrodes are driven by the voltage Φ_A and the y electrodes by $-\Phi_A$, where

$$\Phi_A = \frac{(U - V\cos\omega t)}{2} \tag{1}$$

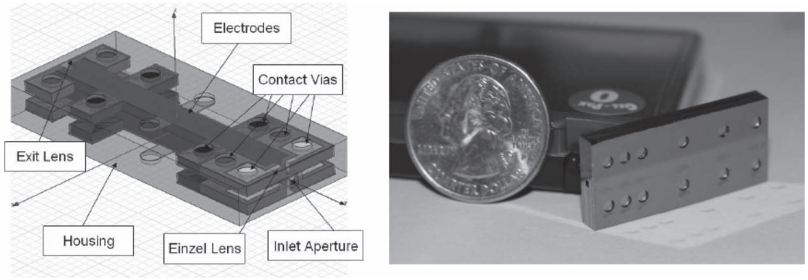

Fig. 2. (Left) Schematic depicting the interior of the device. (Right) Fabricated device placed along a United States of America quarter.

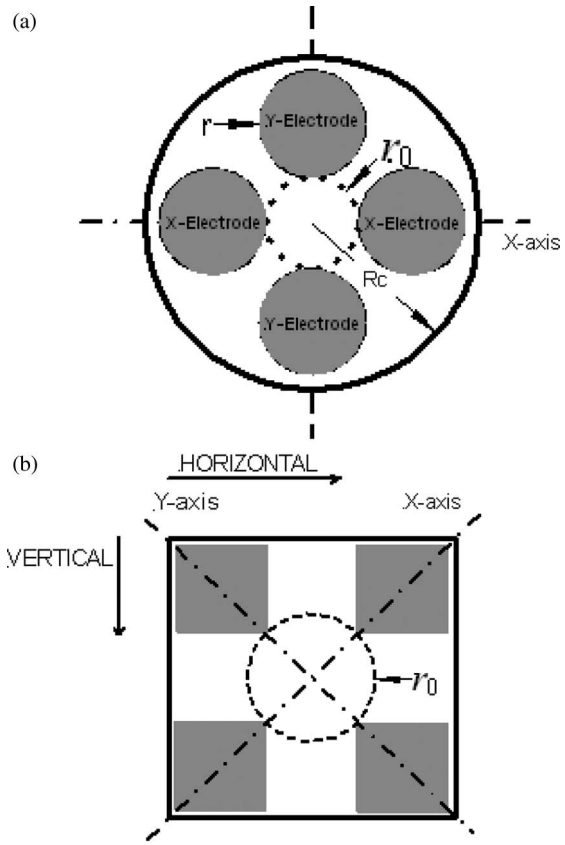

Fig. 3. End views of QMFs constructed from (a) circular electrodes with electrode radius r, field radius r_0, and case radius R_c, and (b) square electrodes, with field radius r_0 showing field axis and electrode displacement directions.

where U is the applied dc voltage, V is the applied ac voltage, ω is the angular frequency, and t is the time.

For a QMF constructed with hyperbolic electrodes, a quadrupole voltage distribution results, producing an electric field that linearly increases with increasing displacement from the central axis and is independent in x and y and invariant in z. With nonhyperbolic electrodes (circular and square), the resultant voltage potential distribution is more complex, consisting of a quadrupole and higher order terms. This can be represented [3], [4] by

$$\Phi(x,y) = \sum_{N=0}^{\infty} \frac{A_N \Phi_N}{r_o^N} \tag{2}$$

$$= \frac{A_0\Phi_0}{r_o^0} + \frac{A_1\Phi_1}{r_o^1} + \frac{A_2\Phi_2}{r_o^2} + \frac{A_3\Phi_3}{r_o^3} + \cdots + \tag{3}$$

where A_N is the amplitude of the multipole Φ_N consisting of 2N poles, with $A_0\,\Phi_0$ defining the offset potential, $A_1\,\Phi_1$ defining the dipole potential, $A_2\,\Phi_2$ defining the quadrupole potential, $A_3\,\Phi_3$ defining the hexapole potential, and continuing thereon. An optimally constructed QMF has fourfold symmetry, and only multipole terms, where $N = 4n + 2$ for $n = 0, 1, 2, 3, \ldots$, contribute to the field.

The exact values of the multipole coefficients are dependent on the electrode geometry [3], which, in turn, determines the closeness of the performance to that obtained with hyperbolic electrodes [4], [6]. For both circular- and square-electrode geometries, the physical arrangement is fourfold symmetric and, provided that perfect electrode alignment is achieved, results in only terms $N = 4n + 2$, where $n = 0, 1, 2, 3, \ldots$.

For geometry that is invariant in the z-axis and ignoring fringing fields, a 2-D model can be used to investigate the behavior of ions in the QMF. If small perturbations of the ions are considered, it can be assumed that the x and y electric fields are decoupled. Therefore, Newton's second law of motion can be used to determine the motion of the ions and results in the following two equations:

$$m\frac{d^2x}{dt^2} = eE_x \tag{4}$$

$$m\frac{d^2y}{dt^2} = eE_y \tag{5}$$

where m is the mass of the ion, e is the charge on the ion, and E_y and E_x are the instantaneous electric field components in the x- and y-axis, respectively.

A major contributory factor to achieving a high-resolution instrument is the number of RF cycles that an ion experiences during its passage through the QMF [1]. This is dependent on a number of factors and can be defined by

$$N_{\mathrm{rf}} = fL\sqrt{\frac{m}{2E_z}} \tag{6}$$

where N_{rf} is the number of RF cycles that the ion experiences, f is the RF frequency, L is the length of the QMF, m is the mass of the ion, and E_z is the axial ion energy. For operation in stability zone 1, the relationship between resolution and the number of RF cycles that an ion experiences has been obtained from experimental results and can be represented by

$$R = \frac{m}{\Delta m} = \frac{1}{K}N_{\mathrm{rf}}^n \tag{7}$$

where R is the QMF resolution, m is the mass of the ion, Δm is the width of the mass peak at mass m, K is approximately 20

but is dependent on the peak height where the peak width Δm is measured, and n has been found to be approximately 2 [1]. Due to field imperfections, there will be an upper limit to $N_{\rm rf}$, where the preceding relationship commences to deviate. Above this upper limit, the resolution will less rapidly increase before finally saturating at a maximum value. The dynamic range of the resolution with respect to $N_{\rm rf}$ provides an indicator of the quality of the instrument and the resultant electric field [1]. For operation in zone 3, the value of K is much smaller with a typical maximum value of 1.43 [29], [30], resulting in a much greater resolution for a given $N_{\rm rf}$ when compared with zone-1 operation. This increased resolution is due to the increased sharpness of the zone-3 stability region [31]. The a and q values for zone 3 are much larger than those associated with zone 1 and result in higher operating voltages for the same operating frequency. Due to the breakdown characteristics of the oxide layers and the much smaller electrode gaps, the result is a reduced mass range.

III. Simulation and Experimental Techniques

The suite of software known as Poisson/Superfish [32] that is available through public access from LANL [33] was used to solve the fields for the electrode geometries investigated. A text file that contained simple text string primitives and dimensions to define the electrode geometry was generated. This text file acts as a problem definition input for the Automesh module. Automesh processes this file, creating a triangular mesh of the free space between the electrodes. The Poisson module solves the field and generates the multipole coefficients for the geometry. The SF7 field interpolator module produces a user-defined 1600 $\times$ 1600 square grid of field data for the central square aperture. Finally, a custom utility FieldCalc extracts, formats, and creates a field data file in the correct format for use by the QMS2-Field ion trajectory software.

QMS2-ION [10] is an ion source program, which generates the entry conditions for a large number of ions. An ion beam providing uniform illumination centrally positioned and parallel to the field aperture is produced. No account is taken of the relative ionization efficiencies of the different ion types. This information is stored in an ion source file and accessed by the ion trajectory programs. Each ion is arranged to have a random phasing with respect to the RF signal. Trajectories for a minimum of 500 steps across the mass range (see results) with 10^5 ions at each mass step were traced using QMS2-Hyperbolic [10] for the hyperbolic electrodes and QMS2-Field [10] for the circular- and square-electrode devices. The simulation test conditions are shown in Table II, and these apply for all simulations, unless stated otherwise.

The microfabricated QMF was manufactured using MEMS technology to form four 30.6-mm-long square 1 mm $\times$ 1 mm rods, which are oriented such that they had an inscribed diameter of 1.414 mm. The device contains a preliminary housing, the mass filter, and integrated optics (Fig. 2). The MEMS device was mounted on a much larger diameter quadrupole housing assembly (80.6 mm in diameter) for convenience of mounting the quadrupole on a conventionally scaled test assembly.

TABLE II
Computer Simulation Test Conditions
(Electrode Comparison)

QMF PARAMETER	CONDITION
Length	30.6 mm
r_0	0.707 mm
$r/\ r_0$ (Circular)	1.127
Square electrode dimensions	1mm x 1mm
Housing radius (Hyp & Cir)	3.6 r_0
Housing dimensions (square)	3.2 mm x 3.2 mm
Frequency (Zone 1)	4 MHz
Frequency (Zone 3)	2 MHz
Detector radius	0.707 mm
Ion Source	
Ion energy (*E*i)	See results
Ion source radius	0.3 mm
Ion energy spread	0
Ion angular spread	0
Operating tip	
a (zone 1,zone 3)	0.237, 3.16
q (zone 1,zone 3)	0.706, 3.23
Ion species	See results

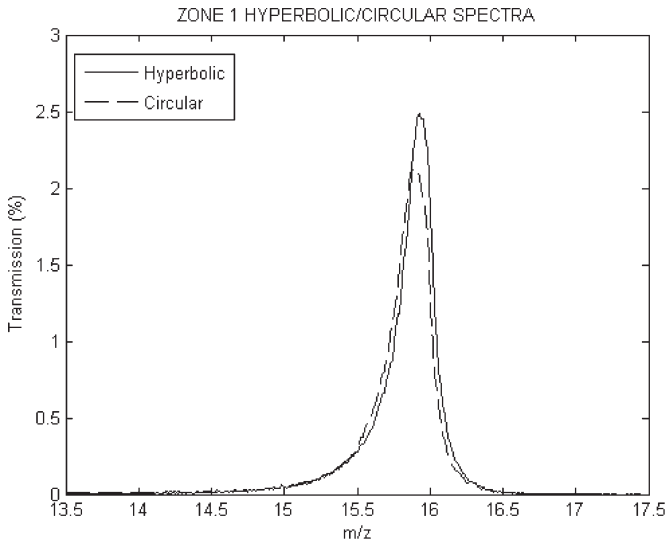

Fig. 4. Computer-simulated mass spectra for O^+ (16 amu) ions with hyperbolic and circular electrodes for operation in stability zone 1.

The QMF was experimentally characterized by measuring the residual gases from a leak of room air into a vacuum chamber in which the quadrupole was mounted on a flange-mounted mass filter configuration. In this configuration, an axial molecular beam ionizer was mounted on the quadrupole housing, which was mounted on a detector housing containing a continuous dynode electron multiplier, which was, in turn, mounted on a feed-through flange. The emissive area of the ionizer was larger (9-mm-diameter ionization region and a 3-mm-diameter extraction lens) than the acceptance of the quadrupole, which had a 2-mm entrance lens positioned 1.00 mm from the front of the device, followed by a 1×1 mm^2 aperture in the microfabricated housing. The integrated optics at the front and

TABLE III
PERFORMANCE CHARACTERISTICS FOR HYPERBOLIC-, CIRCULAR-, AND SQUARE-ELECTRODE QMF (NOTE THAT PH = PEAK HEIGHT.)

	ZONE 1					ZONE 3		
ELECTRODES	HYPERBOLIC	CIRCULAR	SQUARE			SQUARE		
Ion Energy (eV)	3	3	3	5	8	12	18	22
Peak Position (amu)	15.91	15.87	19.25	19.09	18.96	20.13	20.11	20.11
Peak Height (%)	2.46	2.11	5.28	5.80	6.35	0.72	0.81	0.88
Resolution @ 10% PH	22.52	21.26	4.03	3.44	2.95	20.4	13.96	8.29
Resolution @ 50% PH	66.31	54.10	7.68	6.69	5.88	39.73	35.91	30.16
N_{rf}	20.4	20.4	20.4	15.8	12.5	5.1	4.2	3.8

back of the device are positioned 0.1 mm from the housing and the electrodes. The exit lens of the quadrupole positioned 1.00 mm from the end of the device had a 1-mm aperture, followed by a 9-mm-diameter focusing lens and conventionally scaled detector.

This flange-mounted QMF assembly was controlled using a Extrel CMS Merlin data acquisition system and control electronics, with a prototype Ardara Technologies quadrupole power supply operated at 2.0 MHz. Operation in zone 3 required higher ion energies than that in zone 1 for optimum sensitivity. For these zone-3 experiments, ion energy was maintained at 18 eV by biasing the ionization grid to $+18$ V and maintaining the pole bias offset of the quadrupole at 0 V.

IV. RESULT

To provide a performance benchmark for comparison, computer simulations for hyperbolic- and circular-electrode QMFs for operation in zone 1 were first undertaken. They are of the same length and with a comparable field radius to the MEMS device that is the subject of this investigation. The mass spectra for O^+ ions for these two electrode types are shown in Fig. 4, and quantitive performance data are provided in Table III. The two mass spectra are very similar with the exception of the sensitivity (peak height), which is slightly lower for the circular-electrode device. The low resolution and the lack of a significant difference between the two electrode types are attributable to the low number of RF cycles that the ion experiences under the operating conditions tested (20 cycles at 3 eV). The low number of RF cycles experienced by the ion results in a low resolution and the presence of significant low- and high-mass tails. These characteristics result in poor abundance sensitivity, producing an inability to discriminate between closely spaced species.

Fig. 5 shows the simulated mass spectra for zone-1 operation for the square-electrode QMF operated with the same U/V ratio as the round and circular electrodes, with Table III also containing relevant performance data. Several characteristics are apparent when compared with the previous results for hyperbolic and circular devices: The peak height is greater, the peak width is increased, and the low- and high-mass tails are greater, with the peak position shifted to a higher point on the mass scale. The square electrodes have a much-reduced mass filtering performance, resulting in nearly nine times reduction in the 50% PH resolution when compared with hyperbolic electrodes for operation at $E_z = 3$ eV. The shift in the mass scale can largely be attributable to the much-reduced quadrupole coefficient A_2 produced by the square electrodes (A_2 square $= 0.78381$, A_2 circular $= 1.0016$).

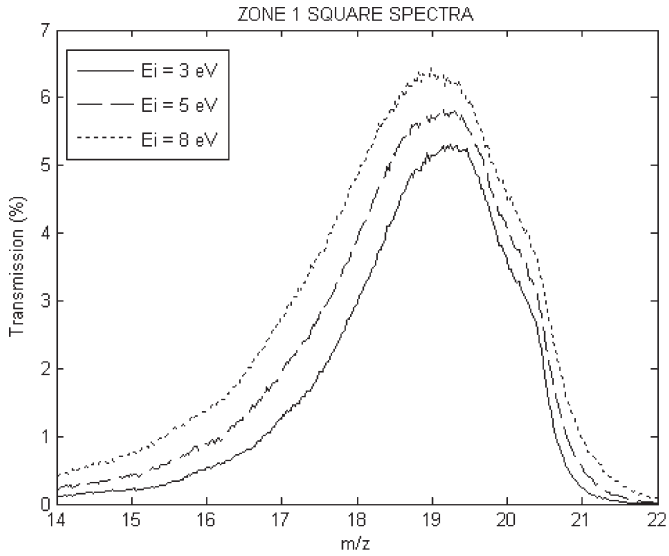

Fig. 5. Computer-simulated mass spectra for O^+ (16 amu) ions with square electrodes for operation in stability zone 1 with the same U/V ratio as Fig. 4 and an uncorrected mass scale.

Computer-simulated mass spectra for square electrodes operating in zone 3 are shown in Fig. 6 and exhibit a better formed mass peak shape when compared with those in zone 1. The low- and high-mass peak tails significantly reduce as does the sensitivity, with the peak position shifted a little higher up the mass scale. Operation in zone 3 requires higher ion energies than that in zone 1 to maximize the transfer of the ions through the increased fringing field in the proximity of the QMF entrance. As a result, ion velocity is increased, and the ions spend less time in the QMF, experiencing a lower number of RF cycles (five cycles at 12 eV for $f = 4$ MHz), compared with zone 1 (20 cycles at 3 eV for $f = 2$ MHz). In spite of the ion exposure to a reduced number of RF cycles, zone 3 still provides improved performance, compared with zone 1.

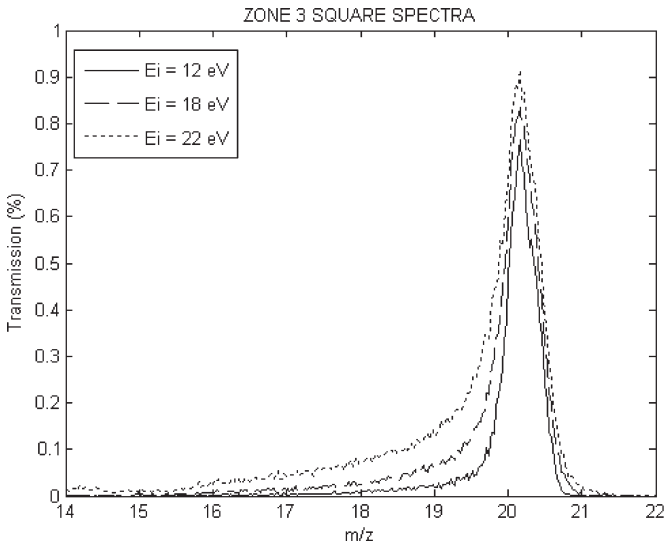

Fig. 6. Computer-simulated mass spectra for O^+ (16 amu) ions with square electrodes for operation in stability zone 3 with uncorrected mass scale.

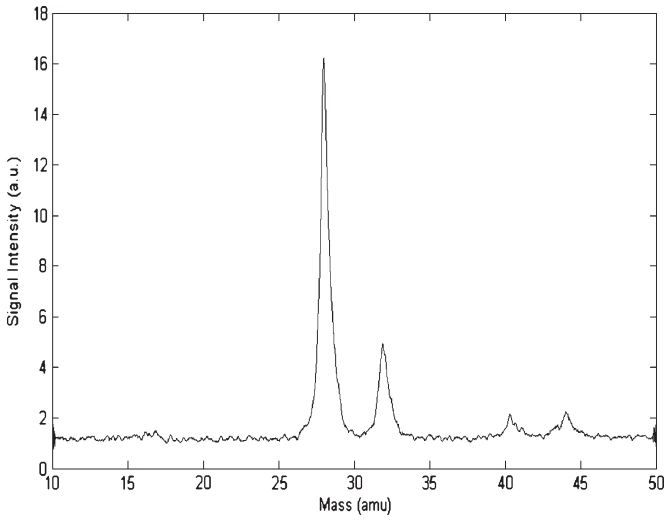

Fig. 7. Square-electrode experimental mass spectra of air for operation in zone 3 for $E_i = 18$ eV.

The square-electrode device achieves a 10% PH resolution of 20.4 at 12 eV for zone-3 operation, compared with 22.52 at 3 eV for hyperbolic electrodes operating in zone 1. These results demonstrate that operation in zone 3 provides a means of improving the resolution of electrode geometries that generate electric fields that are far from the ideal.

Except for very special cases, the QMF is required to discriminate between coexisting species in the sample. Fig. 7 shows experimentally obtained spectra for air when operating in zone 3 with square electrodes. The gain of the experimental system is set to show the peaks for diatomic nitrogen (N_2^+), diatomic oxygen (O_2^+), Ar^+, and CO_2^+. Simulated mass spectra for the same gas sample are shown in Fig. 8. Comparing Fig. 7 with the simulated mass spectra in Fig. 8, we can observe that the simulated data show the correct abundances for the four species simulated. For the experimental results, we observe approximately correct abundances for N_2^+ and O_2^+, with Ar^+

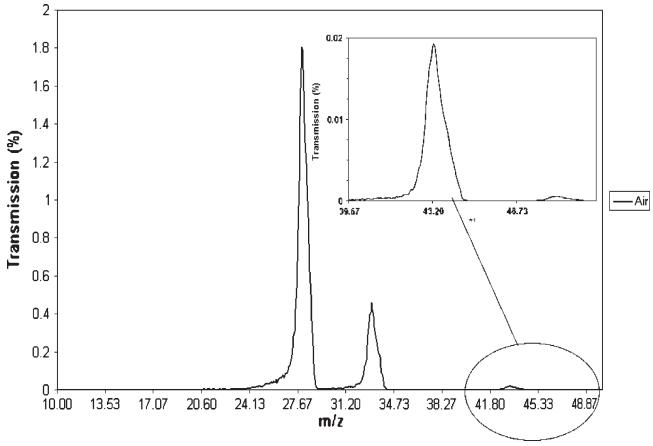

Fig. 8. Square-electrode computer-simulated mass spectra of air for operation in zone 3 with $E_i = 18$ eV.

and CO_2^+ showing higher peaks than expected. The sample abundances of Ar^+ and CO_2^+ are very much smaller than the two major species and therefore more sensitive to background signal levels and electron multiplier noise (signal-to-noise ratio). The measured 10% peak height resolution for N_2^+ is 16.6 (experimental) and 22.6 (simulated), which are of the same order. A well-formed valley between the N_2^+ and O_2^+ peaks is observable in both cases but better defined for the simulated spectra. Low-mass tailing is also more evident for the simulated N_2^+ peak. The differences that do occur are attributable to scan line, baseline, and ion source variations between the experimental equipment and the computer simulation model. In both cases, a mass scale calibration has been performed, and for the simulated data, this was linear across the mass range. There is an increase in the low-mass tail of the major peak, which is possibly due to ion source alignment differences, which are known to have a marked effect on this aspect of performance [8]. There is a very strong correlation between the simulated and experimental results, providing validation of our computer simulation methodology.

The performance obtained for relatively closely spaced species does not completely characterize the performance. This is particularly valid where a relatively short QMF length is employed, resulting in the ions experiencing a small number of RF cycles. This characteristic can result in differences between the low- and high-mass performance due to the differing number of RF cycles experienced across the ion mass range. The effect is accentuated in this case by the very low number of RF cycles experienced at the bottom end of the mass range (five cycles at 18 eV for a 20-amu ion). Use of the QMF over a large mass range enables the mass scan linearity to be quantified and an accurately calibrated mass scan line to be defined. A calibration compound FC-43 was previously used [34], provided the range of species required, and was used to experimentally verify this aspect of performance.

The manufacture of a QMS instrument and, in particular, the QMF component requires careful consideration of the positional tolerances of the electrodes. This is still valid for MEMS-type production processes. The particular characteristics of the MEMS process can result in different combinations

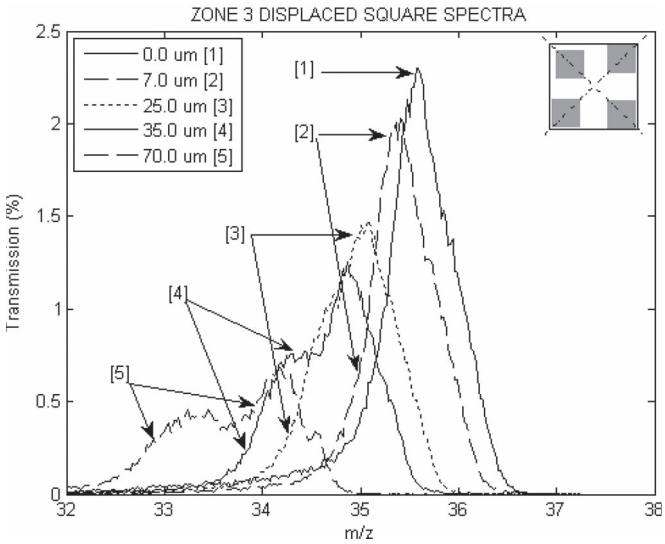

Fig. 9. Computer-simulated zone-3 mass spectra of N_2^+ (28 amu) ions for positional inward displacements of the upper y electrode for $E_i = 18$ eV with uncorrected mass scale. The electrode displacement, which is not to scale, is shown in the inset.

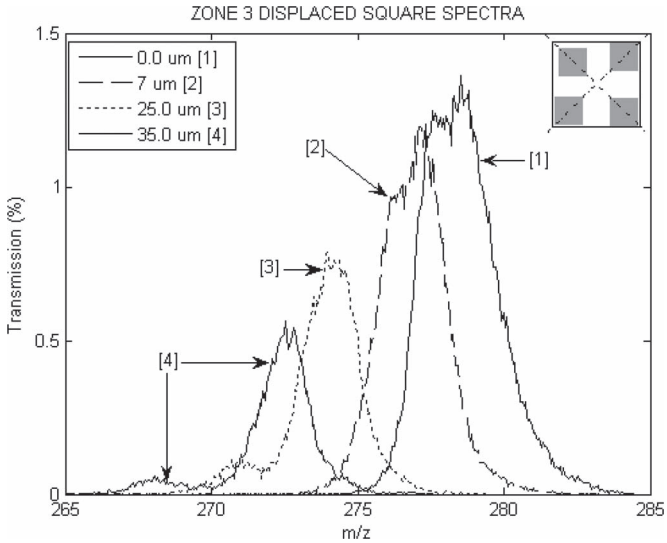

Fig. 10. Computer-simulated zone-3 mass spectra of $C_4F_9^+$ (219 amu) ions for positional inward displacements of the upper y electrode for $E_i = 18$ eV with uncorrected mass scale. The electrode displacement, which is not to scale, is shown in the inset.

of positional tolerances. This, combined with the use of square electrodes, indicates that different tolerance sensitivities may exist and that presently accepted tolerance limits may be different.

Recent literature on the effects of imperfect electrode position [27], [28] has indicated that $+/-0.001r_0$ is an acceptable tolerance limit for the displacement of a single circular electrode of a QMF. This relationship shows that the maximum acceptable value of the electrode tolerance scales with the field aperture of the QMF. In addition, positional tolerances that occur on more than one electrode concurrently, can have a cumulative effect on QMF performance [28]. The absolute tolerance limits associated with MEMS processes are generally smaller, but percentage tolerances can be larger than those achievable using traditional fabrication methods. MEMS devices are usually much smaller with an accompanying smaller field radius. Therefore, if the aforementioned field radius relationship holds, careful control of the tolerance is necessary to achieve adequate performance.

In the first instance, the effects of a single electrode displacement were examined. The manufacturing process used for the construction of the MEMS QMF considered here would not result in this class of electrode displacement due to the two-wafer construction. However, alternative manufacturing processes for achieving miniaturization may well exhibit similar limitations that are found with more conventionally manufactured QMFs. Figs. 9 and 10 show the effects on the mass peak for a single displaced y electrode for two different mass ions N_2^+ (Fig. 8) and $C_4F_9^+$ (Fig. 9), which is a component of FC-43. Table IV provides quantitive performance data for both the ion types for the range of electrode displacements shown in the two figures.

For the lower mass ion N_2^+, as the y electrode is displaced inward on-axis, the mass peak shifts to a lower mass value in response to the increased field strength. There is also an

TABLE IV
PERFORMANCE PARAMETERS FOR DIFFERING INWARD DISPLACEMENTS OF THE y ELECTRODE FOR OPERATION IN ZONE 3 WITH $E_i = 18$ eV

ION TYPE	ELECTRODE DISPLACEMENT (microns)	0	7	25	35
N_2^+ (28 amu) ions	Peak position	35.57	35.36	35.03	34.82
	Peak Height (%)	2.27	1.99	1.45	1.21
	Res 10% PH	22.75	23.68	20.57	18.66
	Res 50% PH	49.18	47.36	35.75	31.09
$C_4F_9^+$ (219 amu) ions	Peak position	278.47	277.17	273.93	272.42
	Peak Height	1.31	1.18	0.76	0.53
	Res 10% PH	52.01	60.39	39.50	68.17
	Res 50% PH	95.50	111.58	126.82	152.87

accompanying decrease in peak transmission and resolution as the electrode displacement increases. The mass peak shape also changes. For displacements below 25 μm, there are only fine detail changes in the mass peak shape, whereas at this value, a shoulder is just visible on the low-mass side of the peak. This shoulder increases in width and moves lower down the peak as the displacement increases until a double peak appears at a displacement of 70 μm.

For the higher mass ions $C_4F_9^+$, the peak transmission decreases. The change in resolution is now less predictable than for the lower mass ions due to the appearance of the precursor peak. The mass peak behavior is more marked with the shoulder emerging at the much smaller displacement of 7 μm, with a precursor peak being observable at a displacement of 35 μm. For both types of ions for outward displacements of the y electrode, we observed the mass peak shift to higher position on the mass scale, with the characteristic shoulder on the low-mass side still appearing at approximately the same electrode displacement. From these results, we determine that, for the lower mass ion, the acceptable maximum displacement equates to a tolerance of $+/-0.0035 \times r_0$, and for the higher mass ion, the acceptable

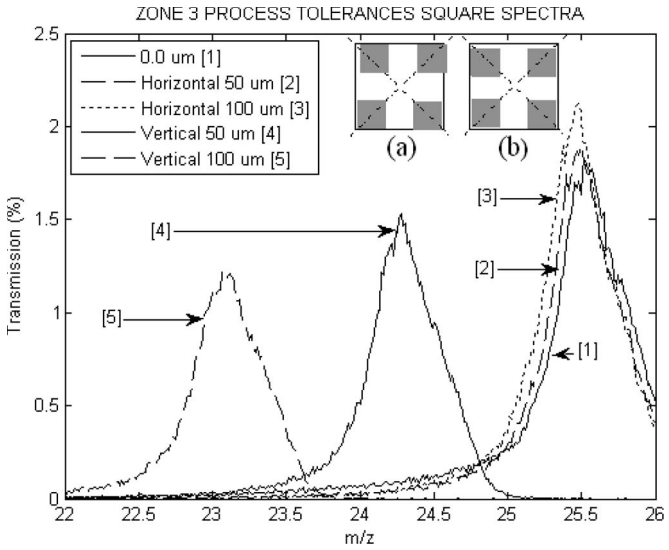

Fig. 11. Computer-simulated zone-3 mass spectra of Ne^+ (20 amu) ions for the horizontal and vertical displacements of the upper electrodes for $E_i = 18$ eV with uncorrected mass scale. The electrode displacements, which are not to scale, are shown in the insets. (a) Horizontal. (b) Vertical.

tolerance is $+/-0.001 \times r_0$. This demonstrates that the maximum acceptable process tolerance for this class of positional error is dependent on the maximum operational mass of the unit.

For the process used in the construction of this MEMS QMF, two of the most dominant misalignments are due to a horizontal shift between the upper and lower electrode pairs during bonding and the differential wafer thickness resulting in a vertical shift of the upper electrodes with respect to the lower electrodes. The bonding process can introduce rotational shifts between the upper and lower electrode pairs, resulting in the horizontal misalignment mentioned and misalignment in the z-axis. The tolerance of this form of misalignment is within $+/-10$ μm, whereas the vertical shift is limited by the wafer thickness tolerance, which is within $+/-5$ μm. The rotational shifts will result in varying degrees of horizontal misalignments along the length of the device. To accurately investigate these shifts would require 3-D simulation software and is outside the scope of this work.

The process tolerance axis is at 45° to the electrode field axis [Fig. 3(b)] and results in compound displacements of the electrodes with respect to the field axis. Fig. 11 shows the effects of these two types of electrode displacements on the resultant mass peak. For the +50- and +100-μm horizontal shifts, there is little observable difference between the mass spectra for a correct electrode placement and the displaced electrodes. The mass peak shifts by small increments to a lower mass position for increasing electrode displacement, and a small progressive increase in peak height is also observable. With this class of process error, both the x and y electrodes are simultaneously displaced in the x and y field axis. The x and y field axis displacements are in the opposite direction and self-compensate, thereby minimizing the resultant effect on the mass peak. A vertical and inward shift of the upper electrodes results in a more marked effect on the mass peak. The mass peak now shifts with greater increments to an increasingly lower mass position. These increments are approximately proportional to the electrode positional shift and are accompanied by a decrease in the peak height (transmission). This type of misalignment results in a compound displacement of both electrodes in both field axes. The x and y field axis displacements are of the same magnitude and same direction for both electrodes. As a result, the effect on the mass peak is cumulative and produces a much greater mass peak shift, and is accompanied by a reduction in transmission. We have observed similar characteristics for circular electrodes.

V. Conclusion

Our experimental and computer simulation techniques have demonstrated that the use of zone-3 operation for a QMF with square electrodes provides improved mass filtering action, compared with that achievable with zone 1. The use of zone 3 enables acceptable performance to be obtained, even though the QMF produces a nonideal electric field and its short length results in the ions being exposed to a relatively low number of RF cycles. The lower quadrupole coefficient (weaker quadrupole field) produced by the square electrodes results in the drive voltage being approximately 1.28 times greater than for a comparable hyperbolic- or circular-electrode device operating under the same conditions. This results in a lower achievable maximum mass for the square-electrode QMF for a given maximum safe operating voltage.

A displacement of a single electrode in the y field axis over a certain limit will result in a precursor before the main mass peak. The acceptable limit of the displacement is determined by the velocity of the ion, which, for a given ion energy, is mass dependent. Therefore, as the mass range is increased, a reduction in the process tolerance is required (with all other operating conditions being the same). The more common process errors, which are a concurrent displacement of both the upper x and y electrodes, produce equal magnitude shifts in both field axes and do not result in a precursor over the range of displacements of interest. A mass scale calibration will negate the effects of the observable mass peak shift that do occur. The expected range of the dominant process tolerances does not adversely affect the achievable performance of the QMF.

References

[1] P. H. Dawson, "Principles of operation," in *Quadrupole Mass Spectrometry and Its Applications*. Amsterdam, The Netherlands: Elsevier, 1976, pp. 9–64.

[2] R. E. March and J. F. J. Todd, "Theory of quadrupole instruments," in *Quadrupole Ion Trap Mass Spectrometry*, J. D. Winefordner, Ed., 2nd ed. Hoboken, NJ: Wiley, 2005, pp. 34–50.

[3] M. Szilagyi, "Determination of electric and magnetic fields," in *Electron and Ion Optics*, I. Brodie and J. J. Muray, Eds. New York: Plenum Press, 1988.

[4] D. J. Douglas and N. V. Konenkov, "Influence of the 6th and 10th spatial harmonic on the peak shape of a quadrupole mass filter with round rods," *Rapid Commun. Mass Spectrom.*, vol. 16, no. 15, pp. 1425–1431, Aug. 2002.

[5] J. Schulte, P. V. Shevchenko, and A. V. Radchik, "Nonlinear field effects in quadrupole mass filters," *Rev. Sci. Instrum.*, vol. 70, no. 9, pp. 3566–3571, Sep. 1999.

[6] I. E. Dayton, F. C. Shoemaker, and R. F. Mozley, "The measurement of two-dimensional fields—Part 2: Study of a quadrupole magnet," *Rev. Sci. Instrum.*, vol. 25, no. 5, p. 485, May 1954.

[7] D. R. Denison, "Operating parameters of a quadrupole in a grounded cylindrical housing," *J. Vac. Sci. Technol.*, vol. 8, no. 1, pp. 485–489, Jan. 1971.
[8] J. R. Gibson and S. Taylor, "Numerical investigation of the effect of electrode size on the behavior of quadrupole mass filters," *Rapid Commun. Mass Spectrom.*, vol. 15, no. 20, pp. 1960–1964, Oct. 2001.
[9] J. R. Gibson and S. Taylor, "Asymmetrical features of mass spectral peaks produced by quadrupole mass filters," *Rapid Commun. Mass Spectrom.*, vol. 17, no. 10, pp. 1051–1055, May 2003.
[10] T. J. Hogan and S. Taylor, "Performance simulation of a quadrupole mass filter operating in the first and third stability zones," *IEEE Trans. Instrum. Meas.*, vol. 57, no. 3, pp. 498–508, Mar. 2008.
[11] E. R. Badman and R. G. Cooks, "Miniature mass analysers," *J. Mass Spectrom.*, vol. 35, no. 6, pp. 659–671, Jun. 2000.
[12] R. A. Syms, T. J. Tate, M. M. Ahmed, and S. Taylor, "Design of a microengineered electrostatic quadrupole lens," *IEEE Trans. Electron Devices*, vol. 45, no. 11, pp. 2304–2311, Nov. 1998.
[13] S. Taylor, B. Srigengan, J. R. Gibson, D. Tindall, R. Syms, T. Tate, and M. Ahmed, "A miniature mass spectrometer for chemical and biological sensing," in *Proc. SPIE-Int. Soc. Opt. Eng.*, 2000, vol. 4036, pp. 187–193.
[14] M. Geear, R. R. A. Syms, S. Wright, and A. S. Holmes, "Monolithic MEMS quadrupole mass spectrometers by deep silicon etching," *IEEE J. Microelectromech. Syst.*, vol. 14, no. 5, pp. 1156–1166, Oct. 2005.
[15] S. Wright, R. R. A. Syms, S. O'Prey, G. Hong, and A. S. Holmes, "Comparison of ion coupling strategies for a microengineered quadrupole mass spectrometer," *J. Amer. Soc. Mass Spectrom.*, vol. 20, no. 1, pp. 146–156, Jan. 2009.
[16] L. F. Velásquez-García and A. I. Akinwande, "An out-of-plane MEMS quadrupole for a portable mass spectrometer," in *Proc. 14th Int. Conf. Solid-State Sens., Actuators, Microsyst.*, Lyon, France, Jun. 2007, pp. 2315–2320.
[17] T. Hayashi and N. Sakudo, "Quadrupole field in circular concave electrodes," *Rev. Sci. Instrum.*, vol. 38, no. 7, pp. 958–961, Jul. 1968.
[18] N. Sakudo and T. Hiyashi, "Quadrupole electrodes with flat faces," *Rev. Sci. Instrum.*, vol. 46, no. 8, pp. 1060–1062, Aug. 1975.
[19] C. G. Pearce and D. Halsall, "A quadrupole mass filter with flat electrodes," *J. Mass Spectrom.*, vol. 27, no. 1, pp. 31–41, May 1978.
[20] N. Sillon and R. Baptist, "Micromachined mass spectrometer," *Sens. Actuators B, Chem.*, vol. 83, no. 1–3, pp. 129–137, Mar. 2002.
[21] R. Baptist, "Miniature device for generating a multi-polar field, in particular for filtering of deviating or focusing charged particles," U.S. Patent 6 465 792 B1, Oct. 15, 2002.
[22] P. H. Dawson and M. Meunier, "Some distortions in quadrupole fields and their relation to mass filter performance," *Int. J. Mass Spectrom. Ion Phys.*, vol. 29, no. 3, pp. 269–299, Mar. 1979.
[23] J. R. Gibson, S. Taylor, and J. H. Leck, "Detailed simulation of mass spectra for quadrupole mass spectrometer systems," *J. Vac. Sci. Technol. A, Vac. Surf. Films*, vol. 18, no. 1, pp. 237–243, Jan. 2000.
[24] J. R. Gibson and S. Taylor, "Prediction of quadrupole mass filter performance for hyperbolic and circular cross section electrodes," *Rapid Commun. Mass Spectrom.*, vol. 14, no. 18, pp. 1669–1673, Sep. 2000.
[25] K. Cheung, L. F. Velásquez-García, and A. I. Akinwande, "Fully batch-fabricated linear quadrupole mass filters," in *Proc. IEEE Solid-State Sens., Actuators, Microsyst. Workshop Tech. Dig.*, Hilton Head Island, SC, 2008, pp. 316–319.
[26] J. J. Tunstall, A. C. C. Voo, and S. Taylor, "Computer simulation of the mass filter for a finite length quadrupole," *Rapid Commun. Mass Spectrom.*, vol. 11, no. 2, pp. 184–188, Jan. 1997.
[27] S. Taylor and J. Gibson, "Prediction of the effects of the imperfect construction of a QMS filter," *J. Mass Spectrom.*, vol. 43, no. 5, pp. 609–616, May 2008.
[28] T. J. Hogan and S. Taylor, "Effects of mechanical tolerances on QMF performance for operation in the third stability zone," *IEEE Trans. Instrum. Meas.*, published under forthcoming papers.
[29] Z. Du, D. J. Douglas, and N. Konenkov, "Elemental analysis with quadrupole mass filters operated in higher stability regions," *J. Anal. At. Spectrom.*, vol. 14, no. 8, pp. 1111–1119, 1999.
[30] L. F. Velásquez-García, K. Cheung, and A. I. Akinwande, "An application of 3-D MEMS packaging: Out-of-plane quadrupole mass filters," *J. Microelectromech. Syst.*, vol. 17, no. 6, pp. 1430–1438, Dec. 2008.
[31] P. H. Dawson, "Higher zones of stability for the quadrupole mass filter," *J. Vac. Sci. Technol.*, vol. 11, no. 6, pp. 1151–1153, Nov. 1974.
[32] F. L. Krawczyk, J. H. Billen, R. D. Ryne, H. Takeda, and L. M. Young, "The Los Alamos accelerator code group," in *Proc. IEEE Particle Accelerator Conf.*, 1995, vol. 4, pp. 2306–2308.
[33] Poisson/Superfish, LANL. [Online]. Available: http://laacg1.lanl.gov/laacg/services/download_sf.phtml
[34] T. J. Hogan, S. Taylor, K. Cheung, L. F. Velásquez-García, and A. I. Akinwande, "Simulation of a square electrode MEMS quadrupole mass filter operating in stability zones 1 and 3," in *Proc. 56TH ASMS Conf. Mass Spectrom. Allied Topics*, Denver, CO, Jun. 1–5, 2008.

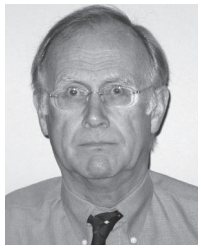

Thomas J. Hogan (M'09) received the qualifications for Chartered Engineer (electrical and electronic) from Hendon College of Technology (now Middlesex University), London, U.K., in 1971 and the M.Sc. degree in microelectronics from the University of Bolton, Bolton, U.K., and the University of Northumbria, Newcastle, U.K., in 2004.

He is currently an External Student with the Department of Electrical Engineering and Electronics, University of Liverpool, Liverpool, U.K. He is also an independent Consultant Engineer in Cambridge, U.K., and has acted for a number of blue chip and startup companies on the design of bespoke electronic and software systems, including computer graphics, satellite imaging, scientific instrumentation, and laser systems. His professional interests include instrumentation, automotive, and embedded control. His research interests include numerical simulation, instrumentation, and reversible computing.

Mr. Hogan is also a European Engineer and a member of The Institute of Engineering and Technology (U.K.).

Stephen Taylor received the B.Sc. degree from Imperial College, London, U.K., in 1978, and the M.Eng. and Ph.D. degrees from the University of Liverpool, Liverpool, U.K., in 1983 and 1988, respectively.

He is currently a Reader with the Department of Electrical Engineering and Electronics, University of Liverpool. He has acted as consultant to several U.K. companies and is a Director of a University start-up company. In 1995, he invented and codeveloped the (then) world's smallest mass spectrometer and the first to be microengineered in silicon. He is a Guest Editor for the *Journal of American Society for Mass Spectrometry*. His teaching duties include courses in electromagnetics and microelectromechanical systems design. He is the author or coauthor of more than 200 papers, patents, or publications in the open scientific literature.

Dr. Taylor is a Fellow of The Institute of Engineering and Technology (FIEE) and the Electrical Research Association. He is a Chartered Engineer. He is a member of the organizing committee for the RGA Users group and a member of the program committee for the Harsh Environment Mass Spectrometry Conference.

Kerry Cheung received the B.S. degree (*magna cum laude*) in applied and engineering physics from Cornell University, Ithaca, NY, in 2003 and the M.S. and Ph.D. degrees in electrical engineering from Massachusetts Institute of Technology (MIT), Cambridge, in 2005 and 2009, respectively.

He is currently a Postdoctoral Associate with the Microsystems Technology Laboratories, MIT, continuing his work on portable mass spectrometry. His research interests are the application of micro- and nanofabrication technologies for MEMS/NEMS sensor development, integrated microsystems, instrument miniaturization, biotechnology, and green technology.

Luis Fernando Velásquez-García (M'09) received the B.S. degree in mechanical engineering (*magna cum laude*) and B.S. degree in civil engineering (*magna cum laude*) from the Universidad de Los Andes, Bogotá, Colombia, in 1998 and 1999, respectively, and the M.S. degree in aeronautics and astronautics and the Ph.D. degree in space propulsion from Massachusetts Institute of Technology (MIT), Cambridge, in 2001 and 2004, respectively.

In 2004, after completing his studies, he became a Postdoctoral Associate with the Microsystems Technology Laboratories, MIT, where he has been a Research Scientist since 2005. He is an expert in micro- and nanofabrication technologies. He has conducted research on micro- and nanotechnology applied to electrospray, silicon-based and carbon-nanotube-based field emission devices, 3-D packaging, portable mass spectrometry, propulsion, and chemical lasers. He is the author of more than 12 journal publications and 26 conference proceeding works. He is the holder of six patents on microelectromechanical systems technologies. His research interests include the application of micro- and nanotechnology to scaled-down multiplexed systems for propulsion, power conversion, manufacturing, and sensing applications.

Dr. Velásquez-García is a member of Sigma Xi and The American Institute of Aeronautics and Astronautics.

Akintunde Ibitayo (Tayo) Akinwande (S'81–M'86–SM'04–F'08) received the B.Sc. degree in electrical and electronic engineering from the University of Ife, Ife, Nigeria, in 1978 and the M.S. and Ph.D. degrees in electrical engineering from Stanford University, Stanford, CA, in 1981 and 1986, respectively.

In 1986, he joined Honeywell International, Inc., Morristown, NJ, where he initially conducted research on GaAs complementary field-effect transistor technology for very high speed and low-power signal processing. He later joined the Si Microstructures Group, where he conducted research on pressure sensors, accelerometers, and thin-film field emission and display devices. In January 1995, he joined the Microsystems Technology Laboratories, Massachusetts Institute of Technology (MIT), Cambridge, where his research focused on microfabrication and electronic devices, with particular emphasis on smart sensors and actuators, intelligent displays, large-area electronics (macroelectronics), field emission and field ionization devices, mass spectrometry, and electric propulsion. He was a Visiting Professor with the Department of Engineering and an Overseas Fellow with Churchill College, Cambridge University, Cambridge, U.K., in 2002 and 2003. He is currently a Professor with the Department of Electrical Engineering and Computer Science, MIT. He is the author of more than 100 journal publications. He is the holder of numerous patents in microelectromechanical systems, electronics on flexible substrates, and display technologies.

Prof. Akinwande is currently a member of the IEEE Nanotechnology Council. He has served on a number of technical program committees for various conferences, including the Device Research Conference, the IEEE International Electron Devices Meeting, the IEEE International Solid-State Circuits Conference, the International Display Research Conference, and the International Vacuum Microelectronics Conference. He was the recipient of the 1996 National Science Foundation CAREER Award.

Randall E. Pedder received the Ph.D. degree in ion trap mass spectrometry from the University of Florida, Gainesville, in 1989.

He has worked for Finnegan MAT, Inficon, and Extrel before becoming the founder and the Chief Executive Officer of Ardara Technologies L.P., North Huntington, PA, in 2004. Ardara Technologies is a leading provider of custom mass spectrometry components and systems to end users and MS instrument manufacturers alike. He has authored or coauthored several papers and book chapters in the scientific literature. He is the holder of three patents. He is a consultant to numerous major companies in the mass spectrometry field.

Dr. Pedder is a member of the American Society for Mass Spectrometry and of the organizing committee for the Harsh Environment Mass Spectrometry Workshop.